NUWC-NPT Technical Report 11,762
1 September 2006

Bending Behavior of Plain-Woven Fabric Air Beams: Fluid-Structure Interaction Approach

Paul V. Cavallaro
Ranges, Engineering, and Analysis Department

Ali M. Sadegh
The City College of New York

Claudia J. Quigley
U.S. Army Research, Development and Engineering Command

NEWPORT

Naval Undersea Warfare Center Division
Newport, Rhode Island

PREFACE

This report was funded under NUWC Division Newport Assignment Number TD0207, principal investigator Paul V. Cavallaro (Code 70T). The research was conducted in support of the Center of Excellence for Inflatable Composite Structures at the U.S. Army Natick Soldier Center (NSC) in Natick, MA, through Military Interagency Purchase Request Number 6CS6R00319. The NSC project officer is Jean Hampel.

The technical reviewer for this report was Andrew J. Hull (Code 8212).

The authors especially thank Karen Horak of the NSC for coordinating technical discussions and information exchanges with industry, academia, and other DoD agencies; Joseph J. Stace (Code 1512) for conducting the multi-axial fabric tests and extensive data reductions; and Adam Turner of the University of Maine at Orono for providing the high quality fabric material samples that were crucial to obtaining exceptional experimental results.

Reviewed and Approved: 1 September 2006

Harriet L. Coleman

Harriet L. Coleman
Head, Ranges, Engineering, and Analysis Department

REPORT DOCUMENTATION PAGE

Form Approved
OMB No. 0704-0188

1. AGENCY USE ONLY *(Leave blank)*	2. REPORT DATE	3. REPORT TYPE AND DATES COVERED
	1 September 2006	

4. TITLE AND SUBTITLE

Bending Behavior of Plain-Woven Fabric Air Beams: Fluid-Structure Interaction Approach

5. FUNDING NUMBERS

6. AUTHOR(S)

Paul V. Cavallaro, Ali M. Sadegh, Claudia J. Quigley

7. PERFORMING ORGANIZATION NAME(S) AND ADDRESS(ES)

Naval Undersea Warfare Center Division
1176 Howell Street
Newport, RI 02841-1708

8. PERFORMING ORGANIZATION REPORT NUMBER

TR 11,762

9. SPONSORING/MONITORING AGENCY NAME(S) AND ADDRESS(ES)

U.S. Army Natick Soldier Center
Kansas Street
Natick, MA 01760-5018

10. SPONSORING/MONITORING AGENCY REPORT NUMBER

11. SUPPLEMENTARY NOTES

12a. DISTRIBUTION/AVAILABILITY STATEMENT

Approved for public release; distribution is unlimited.

12b. DISTRIBUTION CODE

13. ABSTRACT (Maximum 200 words)

A swatch of plain-woven fabric was subjected to biaxial tests to determine its material characteristics. The stress-strain relationships of the fabric were determined and used directly in finite element models of an air beam that was assumed to be constructed of the same fabric and subjected to inflation and bending events. The structural responses to these events were obtained using the *ABAQUS*/Explicit finite element solver for a range of pressures, including those considered to be typical in safe operations of air-inflated structures. The models accounted for the fluid-structure interactions between the air and the fabric. The air was treated as a compressible fluid in accordance with the Ideal Gas Law and was subjected to adiabatic constraints during bending. The fabric was represented with membrane elements. Several constitutive cases, including linear elasticity and hyperelasticity, were studied. The bending behavior for each constitutive case is presented, followed by a discussion of the use and limitations of the cases.

14. SUBJECT TERMS

Inflated Structures
Air Beams
Crimp Interchange
Finite Element Analysis
Plain-Woven Fabric
Explicit Methods

15. NUMBER OF PAGES
34

16. PRICE CODE

17. SECURITY CLASSIFICATION OF REPORT	18. SECURITY CLASSIFICATION OF THIS PAGE	19. SECURITY CLASSIFICATION OF ABSTRACT	20. LIMITATION OF ABSTRACT
Unclassified	Unclassified	Unclassified	SAR

TABLE OF CONTENTS

LIST OF ILLUSTRATIONS

LIST OF ILLUSTRATIONS (Cont'd)

Figure **Page**

LIST OF TABLES

Table **Page**

LIST OF ABBREVIATIONS, ACRONYMS, AND SYMBOLS

A_{warp}	Warp yarn cross-sectional area
A_{weft}	Weft yarn cross-sectional area
C	Crimp content (%)
C_{i0}	Temperature dependent material parameter
D_i	Temperature dependent material parameter
E	Elastic modulus
E'_{tan}	Instantaneous tangent modulus
E_{dis}	Viscous dissipation energy
E_{int}	Internal energy
$E_{kinetic}$	Kinetic energy
EOS	Equation of state
E_{strain}	Strain energy
E_{tan}	Tangent modulus
F_{react}	Sum of load point reaction forces
G	Shear modulus
$\bar{I}_1$	First deviatoric strain
J^{el}	Elastic volume ratio
L_{fabric}	Reference length of yarn in fabric
L_{yarn}	Length of yarn extracted from fabric
M_w	Molecular weight
$M_{wrinkle}$	Wrinkling moment
N	Material parameter
NSC	U.S. Army Natick Soldier Center
NUWC	Naval Undersea Warfare Center
P	Inflation pressure
P_A	Ambient pressure
PdV-work	Air compressibility
r	Radius of cylinder
R	Gas constant
$\tilde{R}$	Universal gas constant
S	Stress ratio
S^C	Converged stress ratio
U	Strain energy per volume
V	Air volume
W_{ext}	External work done
YDR	Yarn density ratio
γ	Shear strain
Δ	Change between bending and inflation end states
δ_{load_pt}	Load point displacement
δ_{mid}	Mid-span deflection
ε	Strain due to equi-biaxial extension
ξ	Crimp ratio
θ	Current temperature

θ^Z	Absolute zero temperature
μ_0	Initial hyperelastic shear modulus
ν	Poisson's ratio
ρ	Density of air
σ_{warp}	Warp direction stress
σ_{weft}	Weft direction stress
τ	Shear stress

BENDING BEHAVIOR OF PLAIN-WOVEN FABRIC AIR BEAMS: FLUID-STRUCTURE INTERACTION APPROACH

INTRODUCTION

This report extends previous experimental and numerical modeling efforts[1, 2] that addressed the bending behavior of uncoated, plain-woven fabric air beams. The prior efforts showed that the elastic and shear moduli were independent of the elastic modulus of the yarns but were dependent upon inflation pressure, fabric construction, and crimp interchange.[2] The models also treated the stiffening influence of inflation pressure on only the constitutive properties of the fabric. Changes in pressure and volume were not considered.

The objectives of the current research were to (1) characterize the mechanical properties of a structural fabric through swatch-level tests by using a combined biaxial tension and shear test fixture,[3] (2) input the resulting biaxial stress-strain behavior directly into air beam finite element models, (3) predict the bending behavior of the air beam while accounting for fluid-structure interactions (i.e., air compressibility), (4) identify the limitations of using linear elasticity and hyperelasticity to represent the fabric constitutive behavior, and (5) assess the contributions of air compressibility (as a form of PdV-work) and fabric strain energy on air beam bending behavior.

A swatch of plain-woven fabric was subjected to biaxial tests to characterize its mechanical properties. The stress-strain relations of the fabric were determined and used directly in finite element models of an air beam that was assumed to be constructed with the same fabric. The structural responses to inflation and bending events were obtained using the ABAQUS/Explicit[4] finite element solver for a range of pressures, including those considered to be typical in safe operations of air-inflated structures. The models accounted for the fluid-structure interactions between the air and the fabric. The air was treated as a compressible fluid in accordance with the Ideal Gas Law and was subjected to adiabatic constraints during bending. The fabric was represented with membrane elements. Several constitutive cases, including linear elasticity and hyperelasticity, were studied. The bending behavior for each constitutive case is presented, followed by a discussion of the use and limitations of the cases.

DESCRIPTION OF PLAIN-WOVEN FABRIC

The fabric was a dense, high-quality, uncoated, plain-woven polyester as shown in figure 1 and is commercially used in the construction of fire hoses. The warp yarns were aligned in the longitudinal direction of the fire hose and the weft yarns, orthogonal to the warp yarns, were aligned in the hoop direction. Specific details at the yarn and fabric levels were measured, using reverse engineering, and are reported in table 1.

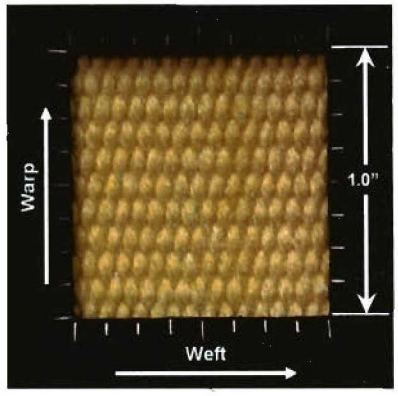

Figure 1. Image of Plain-Woven Polyester Fabric

Table 1. Details of the Plain-Woven Polyester at the Yarn and Fabric Levels

Characteristic	Description
Warp Yarns	Polyester 5 bundles 2 twists/in. Cross-section area = 0.00105 in.^{2}
Weft Yarns	Polyester 1 bundle 2 twists/in. Cross-section area = 0.00153 in.^{2}
Fabric Densities	Warp yarns per unit circumference = 15 yarns/in. Weft yarns per unit length of air beam = 11 yarns/in. Yarn density ratio (YDR) = 0.73
Crimp Measurements	C_{warp} = 15.0% C_{weft} = 3.1% $\zeta = C_{warp}/C_{weft}$ = 0.21

The crimp ratio C is defined as the waviness of the yarns as obtained by equation (1):

$$C = \frac{L_{yarn} - L_{fabric}}{L_{fabric}}, \tag{1}$$

where L_{fabric} is the measured length of a yarn in its fabric state and L_{yarn} is the length of that same yarn after it has been extracted from the fabric and straightened out. It was particularly noted that the fabric was engineered with different crimp amounts between the two yarn families. The crimp content of the warp yarns was nearly five times greater than that of the weft yarns. The yarn density ratio YDR was defined as the number of weft (hoop) yarns per unit beam length divided by the number of warp (longitudinal) yarns per unit circumference.

FABRIC STRESS-STRAIN BEHAVIOR—EXPERIMENT

For pressurized cylindrical beams of radius r, it can readily be shown from equilibrium that the stress ratio S (defined as the ratio of hoop stress per unit beam length to the longitudinal stress per unit circumference) is 2:1, as shown in figure 2. Therefore, to properly characterize the stress-strain behavior of the fabric about a given pressurized state, fabric samples must be tested under biaxial loading conditions that enforce $S = 2$. This ratio holds only for the inflated state and is not applicable to pressurized cylinders subjected to external loads.

The authors did not have access to a combined biaxial and shear test fixture capable of $S = 2$ loading at the time of this research; the equi-biaxial extension test fixture[3] shown in figure 3 was used. For the woven air beam models evaluated in this report, the longitudinal axis was coincident with the warp direction and the hoop axis was coincident with the weft direction (refer to figure 1).

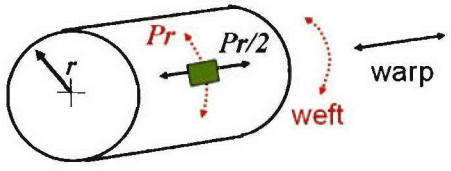

Weft tensile stress per unit length of cylinder = Pr

Warp tensile stress per unit length circumference = $Pr/2$

Figure 2. Stress State in Cylinders Subjected to Internal Pressure

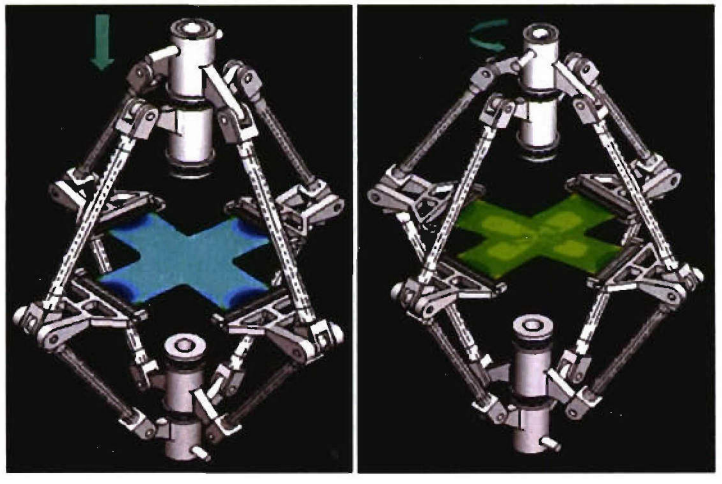

Figure 3. Combined Multi-Axial and Shear Test Fixture (U.S. Patent No. 6,860,156)

A swatch of the polyester fabric, of the dimensions given in figure 4, was subjected to a series of uniaxial tension, biaxial tension, and combined biaxial tension and shear tests, as illustrated in figure 5.

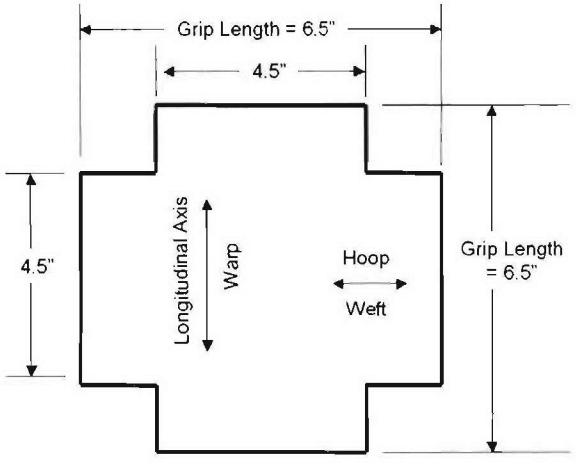

Figure 4. Dimensions of Fabric Swatch Specimen

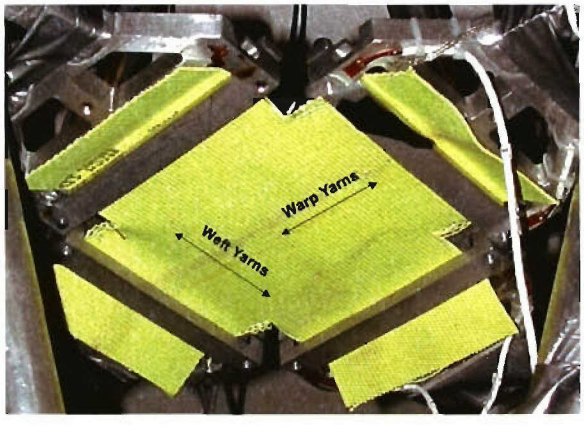

Figure 5. Plain-Woven Polyester Fabric Specimen Subjected to Multi-Axial and Shear Tests

Five experimental stress-strain curves were obtained. These curves corresponded to (1) uniaxial tension along the warp direction, (2) uniaxial tension along the weft direction, (3) biaxial tension along the warp direction, (4) biaxial tension along the weft direction, and (5) planar shear.

The biaxial curves—items 3 and 4 listed above—were obtained from a single test in which the fixture operated in an equi-biaxial extension rather than in the equi-biaxial force mode. The results of the uniaxial and biaxial tests—items 1 through 4 listed above—are plotted in figure 6. Because the maximum fixture load was limited, the fabric was not tested to failure.

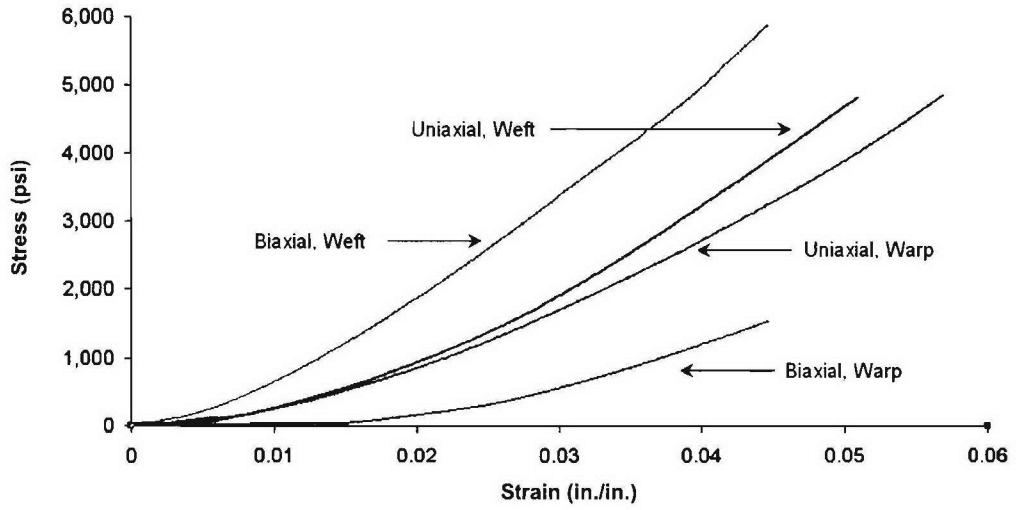

Figure 6. Uniaxial and Biaxial Stress-Strain Curves for Plain-Woven Polyester Fabric

The variation of S resulting from the equi-biaxial extension mode of testing is plotted in figure 7. The result is neither controlled nor constant because the elastic moduli of the fabric were highly nonlinear with respect to extension (and strain). At the maximum equi-biaxial strain ε applied during testing, S is 3.82, nearly twice the required value for properly characterizing the state of stresses in a pressurized cylinder. However, the effects of crimp interchange during the equi-biaxial extension test clearly resulted in pronounced differences between the uniaxial and biaxial curves for a given yarn family. Figure 8 shows the strain-dependent elastic modulus, now referred to as the tangent modulus E_{tan}, along the warp direction as a function of warp stress σ_{warp}.

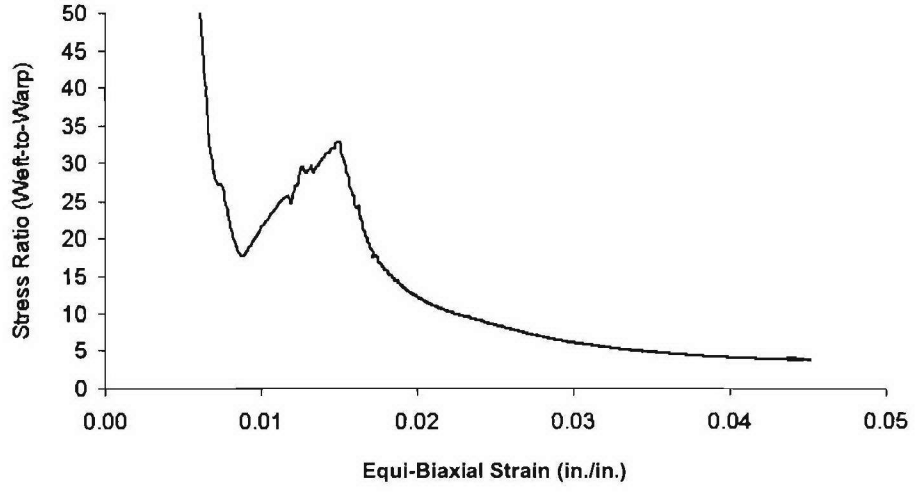

Figure 7. Stress Ratio S vs Equi-Biaxial Strain ε

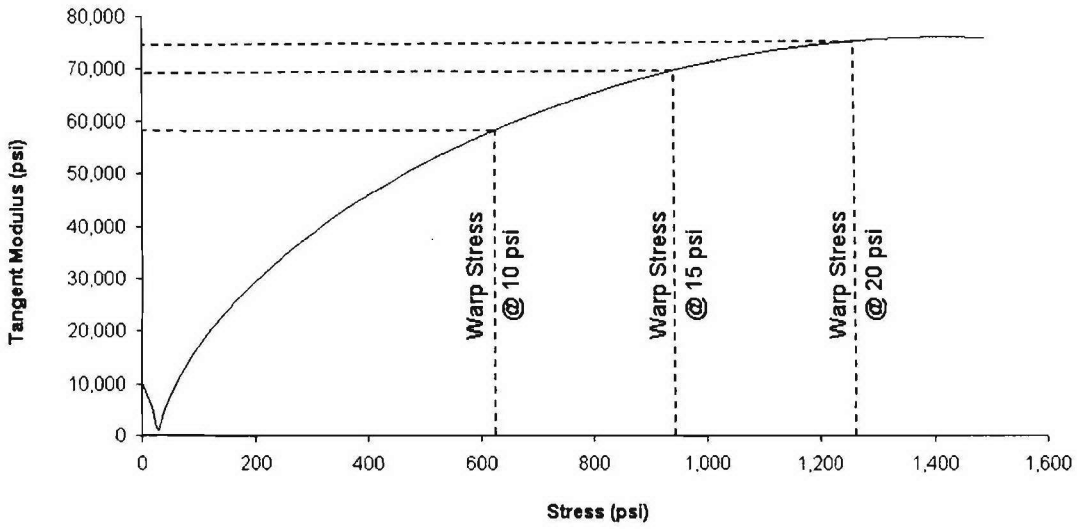

Figure 8. E_{tan} vs σ_{warp} Measured in the Equi-Biaxial Extension Test

The planar shear test was conducted in a constant equi-biaxial extension mode, and σ_{warp} corresponded to that of a 10-psi inflation pressure—a stress of 637 psi, as shown in figure 8. The specimen was loaded to a maximum shearing angle of 10°, and the resulting curve for shear stress τ as a function of shear strain γ is plotted in figure 9.

The shear modulus G, along path $\overline{ab}$ in the direction of increasing γ, was derived by differentiating a polynomial curve fit of figure 9. The resulting shear modulus is plotted in figure 10. Figure 11 illustrates the three distinct regions of shear stiffness, revealed by figure 9, that resulted from kinematic interactions and scissoring deformations between yarn families.

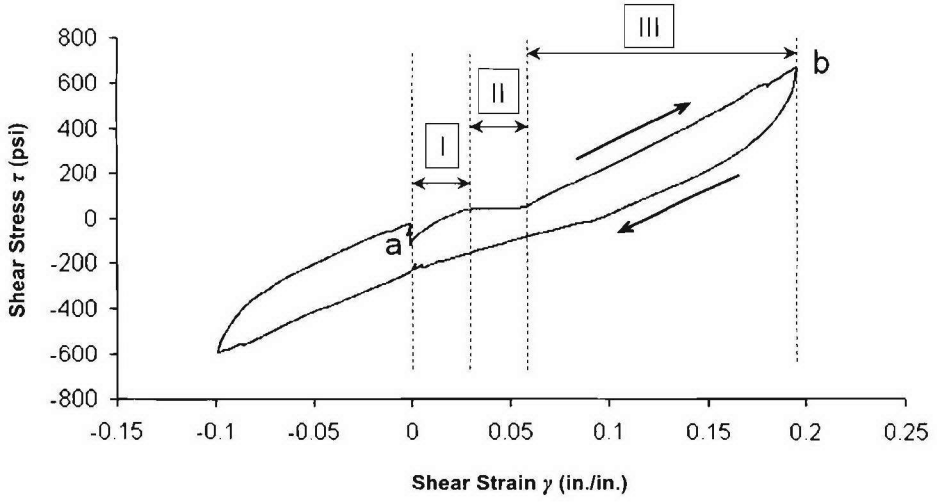

Figure 9. τ vs γ Plotted with P at 10 psi (σ_{warp} = 637 psi)

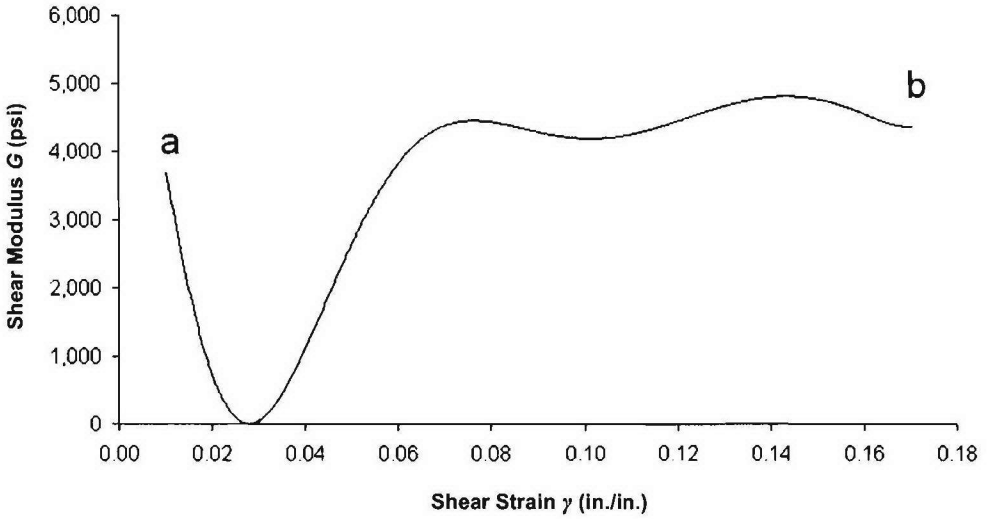

Figure 10. G vs γ with P at 10 psi (σ_{warp} = 637 psi)

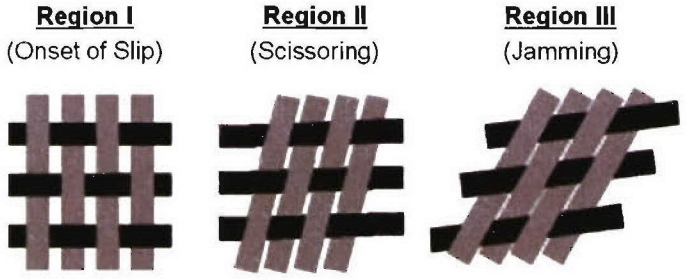

Figure 11. Kinematics of Shear Deformations in Uncoated Plain-Woven Fabrics

Referring to region I in figure 9, G was initially governed by compaction forces between the yarns at the crossover points because of the biaxial tensile stresses. As γ increased, yarn slip initiated, and at γ equal to approximately 0.03 in./in., G declined to practically zero. At this strain, rotations between yarn families were met with no appreciable resistance. Upon further increase of γ into region II, G increased as the gaps between yarn families diminished, and the onset of shear jamming occurred.

Region III is known as the shear jamming state. The onset of shear jamming, which can be determined through geometric models,[5] is related to the maximum number of weft yarns that can be woven into the fabric for a given warp yarn size and spacing. The shearing behavior of this fabric was consistent with the numerical model and test results of the plain-woven fabric investigated in Cavallaro et al.[2]

AIR BEAM FINITE ELEMENT MODELS

The air beams modeled in the effort described in this report were 98 inches long, had a nominal 4.0-inch diameter, and were subjected to four-point bending as shown in figure 12. Although a thin urethane bladder is typically used to line the inner surface of air beams to prevent air leakage through the fabric, it is considered nonstructural. Therefore, such a bladder was not included in the models described here. The models were developed with Altair's HyperWorks[6] pre- and post-processor and the ABAQUS/Explicit solver.[4] This solver was used to capture the pressure-volume behavior of the internal air, transverse shear deformations from bending, geometric nonlinearities due to large deformations, material nonlinearities (for the hyperelastic material models), localized wrinkling, and surface-to-surface contact kinematics.

The fabric was idealized as being incapable of developing bending strain energy and was discretized using membrane elements. However, strain energies associated with extension and shearing deformations were captured. The computation of the membrane element thickness was based on an analogous homogeneous cylinder with an outer diameter of 4.00 inches and a cross-sectional area equivalent to the sum of the warp (axial) yarn areas. The resulting thickness was 0.016 inch. Rigid saddles that were 4.00 inches long and 4.27 inches in inner diameter, as shown in figure 12, were used as the load points (upper saddles) and support points (lower saddles). Full surface-to-surface contact definitions were included between the fabric and saddle elements.

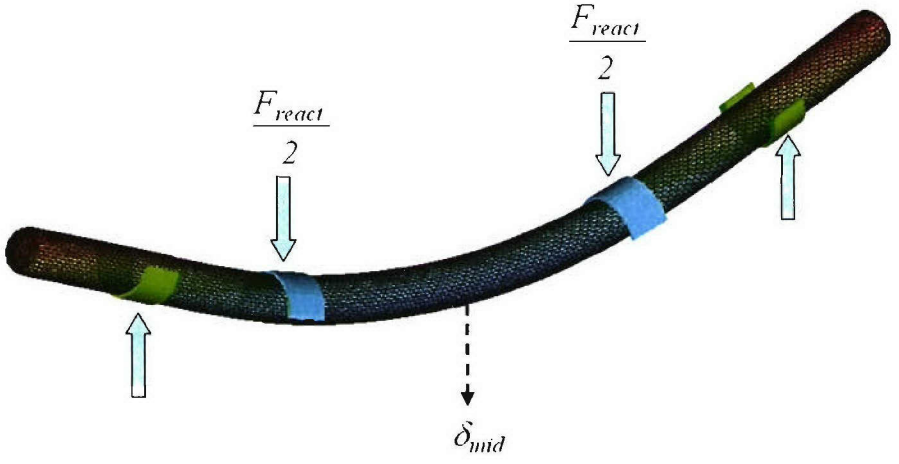

Figure 12. Air Beam Finite Element Model Subjected to Four-Point Bending

The models were loaded by enforcing a lateral displacement δ_{load_pt} of 6.00 inches (1.5 times the diameter) at both load points. The support points were restricted from translating in all directions. All the saddles were allowed to rotate so that the lateral reaction force vectors remained normal to the air beam at all times (i.e., follower mode). A zero coefficient of friction was used at all contact surfaces so that relative slip between the air beam and saddles occurred without restriction. The distance between support point centerlines was 72.0 inches, and the distance between loading point centerlines was 37.0 inches.

To model the fluid-structure interactions of the internal air and surrounding fabric, a pressurized cavity was defined along the inside surface of the fabric material. The cavity and its enclosing surface were used to apply the internal pressure P directly to the membrane (fabric) elements and to define the volume of air contained by the cavity within the air beam. The internal air was modeled as a compressible (pneumatic) fluid that satisfied the ideal gas equation of state (EOS) as described in appendix A. This EOS assumed that compressibility of the air occurred adiabatically; that is, no heat transfer was permitted across the boundaries between the cavity and the fabric.

The external work W_{ext} done on the air beam during a quasi-static four-point bend test was computed as the area under the total reaction force F_{react} as a function of the enforced load point displacement δ_{load_pt} curve. During the bending step, W_{ext} was equal to the change in the internal energy of the air beam ΔE_{int}. The change in internal energy consisted of the sum of the changes in the fabric strain energy ΔE_{strain}, the kinetic energy of the total system mass $\Delta E_{kinetic}$, the work done by compressing the air $\Delta \int PdV$, and the viscous dissipation energy ΔE_{dis} due to damping. (Note that Δ refers to the change between the bending and inflation end states.) An energy balance was performed as shown in equation (2):

$$W_{ext} = \int F_{react}\, \mathrm{d}\, \delta_{load\_pt} = \Delta E_{int}\,, \tag{2}$$

where

$$\Delta E_{int} = \Delta E_{strain} + \Delta E_{kinetic} + \Delta \int PdV + \Delta E_{dis}\,.$$

Transverse shear deformations[7] arising from the shearing strain γ, as shown in the beam-bending example in figure 13, will cause a reduction in air volume and lead to additional *PdV-work*.

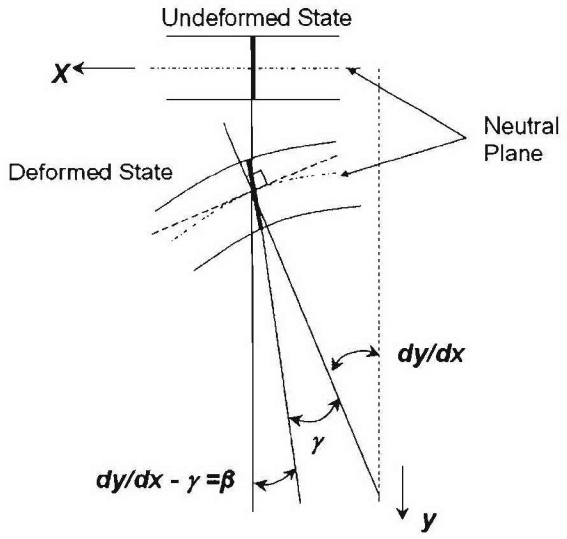

Figure 13. Transverse Shear Deformations During Bending

Although the ABAQUS/Explicit solver was formulated for dynamic problems, it can be used for static applications as well. The analyst must ensure that no modes of the structure are excited for static problems. One method is to ensure that loads are applied slowly and that $\Delta E_{kinetic}$ is small. However, if wrinkling or buckling events were to occur, spikes in the $\Delta E_{kinetic}$ time history curve would develop and allow for easy detection of the event in time. For the effort described here, $\Delta E_{kinetic}$ and ΔE_{dis} were typically observed to make negligible contributions to equation (2).

To evaluate the bending performance of the air beam, a two-step loading process was necessary. First, the cavity was pressurized to the required inflation level during a 2-second time interval. Second, $\delta_{load\_pt} = 6.0$ inches was applied at the load points during a 5-second time interval.

The following section describes the implementation of material-level test results in the air beam bending models. Specifically, the warp direction stress-strain curve taken from the equi-biaxial extension test was used to formulate the linearly elastic and hyperelastic constitutive behaviors assigned to the fabric membrane elements.

ANALYSIS AND RESULTS

CASE 1—LINEAR ELASTICITY, CONSTANT MODULUS FOR ALL PRESSURES

The first case idealized the fabric material as isotropic and linearly elastic. The elastic and shear moduli were, therefore, invariant with inflation pressure. Here, the shear modulus G and elastic modulus E were related through a generalized form of Hooke's Law as

$$G = \frac{E}{2(1+\nu)}, \tag{3}$$

where ν is Poisson's ratio. The value of E was taken as the largest tangent modulus of the warp direction biaxial stress-strain curve E_{tan} (0.1 Mpsi), and ν was set to 0.3 to allow for material compressibility.

The time histories of pressure, internal volume, load-point reaction forces, and energy terms necessary to conduct the energy balance of equation (2) were tracked during the solution. The change in pressure ΔP was plotted as a function of the corresponding change in volume ΔV during bending. The area under this curve was integrated to obtain *PdV-work*.

For this linearly elastic case and the inflation pressures of interest, it was observed that ΔP and ΔV were very small during bending. The results indicated that ΔE_{strain} decreased with increasing P, while *PdV-work* increased with increasing P, as shown in figure 14 for the specified δ_{load_pt}. At pressures below 30 psi, *PdV-work* contributed less than 10% of W_{ext}, and ΔE_{strain}, contributing more than 90%, was the dominant term in the energy balance. However, for inflation pressures of 90 psi and greater, *PdV-work* dominated the energy balance, almost to the exclusion of ΔE_{strain}. The effects of ΔE_{strain} on bending behavior were negligible at these pressures.

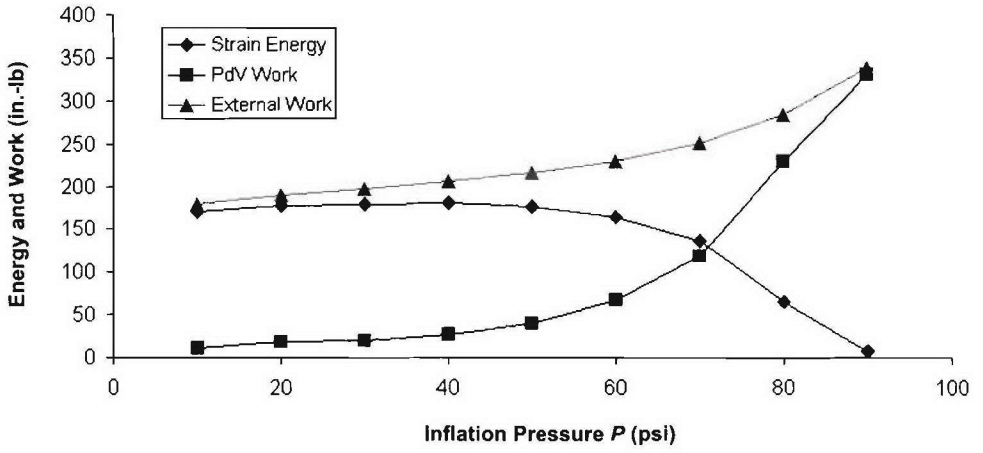

Figure 14. W_{ext}, PdV-work, and ΔE_{strain} vs P for a Linearly Elastic Fabric—Case 1

Figure 15 shows the curves for the total reaction force F_{react} versus δ_{mid} that were plotted for the pressures of interest. For the enforced δ_{load_pt} of 6.0 inches, the occurrence of wrinkling was predicted for pressures of 10 to 40 psi only. The pressures shown in figure 15 for the onset of wrinkling were consistent with the theoretical values obtained from equation (4),

$$M_{wrinkle} = \frac{P\pi r^3}{2}, \tag{4}$$

which is easily derived from a simple stress balance between the inflated and bending stress states in woven air beams.

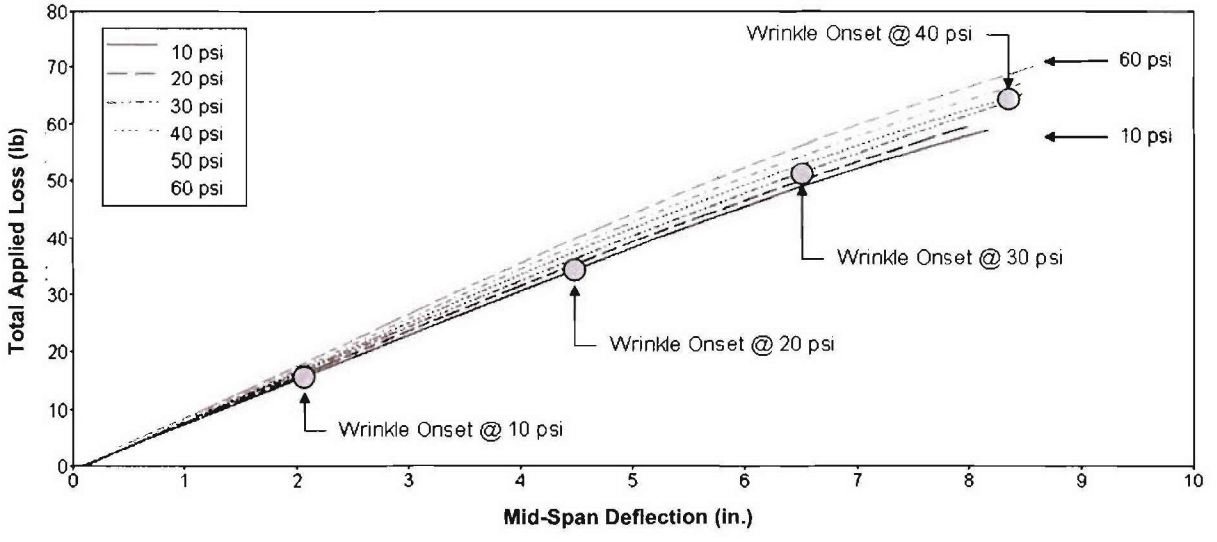

Figure 15. F_{react} vs δ_{mid} Curves for Linear Elastic Material Model with P at 10 to 60 psi —Case 1

In comparison with previous air beam bending experiments, the curves in figure 15 exhibit a moderately weak dependence on P. This effect is attributed to the linearly elastic constitutive relationship of equation (3), whereby G, computed as 38,462 psi, is overly stiff in comparison with the experimental results from figure 10 that reveal a peak G of 4,600 psi, corresponding to P at 10 psi. As a result, no appreciable transverse shearing deformations develop in these models, and ΔV, ΔP and *PdV-work* are inconsequential to the bending behavior. These parameters are summarized for the bending step in table 2.

Table 2. Summary of Pressure, Volume, and Energy Changes During Bending Step—Case 1

P (psi)	ΔP (psi)	ΔV (in.^{3})	$\Delta \int PdV$ (in.-lb)	ΔE_{strain} (in.-lb)
10	0.017	-0.88	8.75	169.64
20	0.024	-0.89	18.20	171.03
30	0.019	-0.56	16.88	179.65
40	0.025	-0.63	25.07	180.65
50	0.036	-0.79	39.25	176.69
60	0.055	-1.07	64.23	164.81

CASE 2—LINEAR ELASTICITY, USE OF INSTANTANEOUS TANGENT MODULI

This case assumed that the fabric material behaved as linearly elastic in accordance with equation (3), but E_{tan} used at each pressure corresponded to the instantaneous tangent modulus E'_{tan} at the state of stress because of inflation at that pressure. In essence, case 2 allowed E_{tan} and G to change with respect to the specific inflation pressure only. From the warp direction biaxial stress-strain curve, the resulting values of σ_{warp} and E'_{tan} are computed for inflation pressures of 10, 15, and 20 psi (see table 3). A 28% increase in E'_{tan} is observed by increasing the inflation pressure from 10 psi to 20 psi.

Table 3. σ_{warp} and E'_{tan} as Functions of P

P (psi)	σ_{warp} (psi)	E'_{tan} (psi)
10	635	58,765
15	952	69,924
20	1,270	75,414

Case 2 was demonstrated for inflation pressures only up to 20 psi because load limitations of the biaxial test fixture prevented characterization of the biaxial warp stress-strain curve beyond 1,500 psi. Hence, E'_{tan} could not be determined for stresses beyond this limit. In addition, the results from this case were valid for only those bending stresses that could be treated as perturbations from the inflated stress states where the tensile and compressive bending behaviors did not deviate from E'_{tan} of the inflated stress state.

The results for the work and energy terms were plotted as functions of inflation pressure in figure 16. The values from case 2 were similar to those from case 1. Curves of F_{react} versus δ_{mid} were plotted in figure 17 for P at 10, 15, and 20 psi. For case 2, wrinkling was predicted for each pressure as shown in figure 17. Changes in the pressure, volume, and energy terms were summarized in table 4.

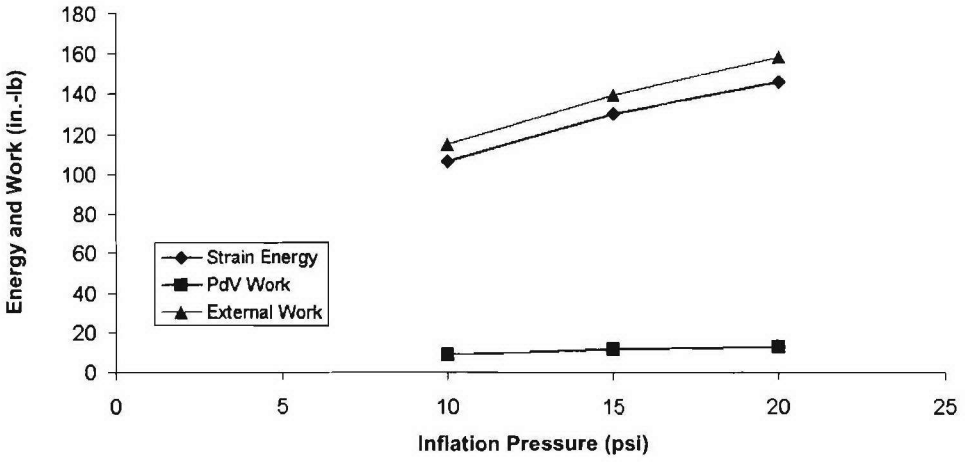

Figure 16. W_{ext}, ΔE_{strain}, and PdV-work vs P for a Linearly Elastic Fabric When E'_{tan} Used with P at 10, 15, and 20 psi—Case 2

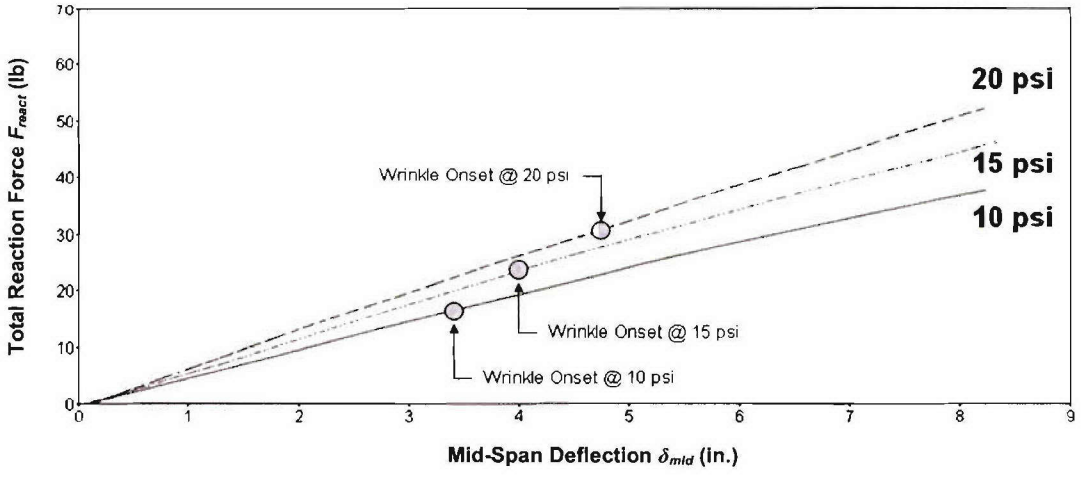

Figure 17. F_{react} vs δ_{mid} for a Linearly Elastic Fabric When E'_{tan} Used with P at 10, 15, and 20 psi—Case 2

Table 4. Summary of Pressure, Volume, and Energy Changes During Bending Step—Case 2

P (psi)	ΔP (psi)	ΔV (in.^{3})	$\Delta \int PdV$ (in.-lb)	ΔE_{strain} (in.-lb)
10	0.017	-0.86	8.65	105.29
15	0.017	-0.73	10.96	127.90
20	0.016	-0.62	12.34	146.25

While further characterization of the fabric constitutive properties (notably, the shear modulus) at pressures beyond 20 psi is necessary, the influences of pressure in case 2 qualitatively followed those observed in previous bending experiments.[1,2] As a result of the changes in both E_{strain} and *PdV-work* with respect to P, plain-woven air beams—in particular—must consider both terms. Plain-woven air beams typically operate at low-pressure levels (less than those for triaxial-woven or braided air beams) because of safety concerns and are, therefore, susceptible to greater transverse shear deformations.

CASE 3—HYPERELASTICITY

This case considered both geometric and material nonlinearities. Here, the full nonlinear constitutive behavior of the plain-woven polyester fabric was idealized as a hyperelastic material. The notable difference between the hyperelastic and materially linearly elastic cases was that hyperelasticity enabled the stiffness of the fabric membrane to change with stresses due to inflation pressure and bending loads.

A hyperelastic strain energy potential was pursued because the uniaxial and biaxial stress-strain curves obtained from swatch-level tests exhibited nonlinear stiffening similar to that of hyperelastic materials. Several strain energy potentials were evaluated using ABAQUS/Explicit to determine the best representation of the warp direction biaxial stress-strain curve. This stress-strain curve specifically dominated the material behavior of the air beam during bending. The reduced polynomial ($N = 3$) strain energy potential,[4] shown in appendix B, provided the best fit for this stress-strain curve and was stable over the entire strain range (i.e., 5%). The initial shear modulus μ_0 was 507.2 psi. The results for the work and energy terms are plotted as functions of inflation pressure in figure 18.

Curves of F_{react} versus δ_{mid} are plotted in figure 19, which clearly shows dependence of the bending behavior on P. However, wrinkling is not predicted at these pressures and δ_{load_pt} because the moments generated are less than required by equation (4). The changes in pressure, volume, and energy terms during the bending step are listed in table 5 as a function of P.

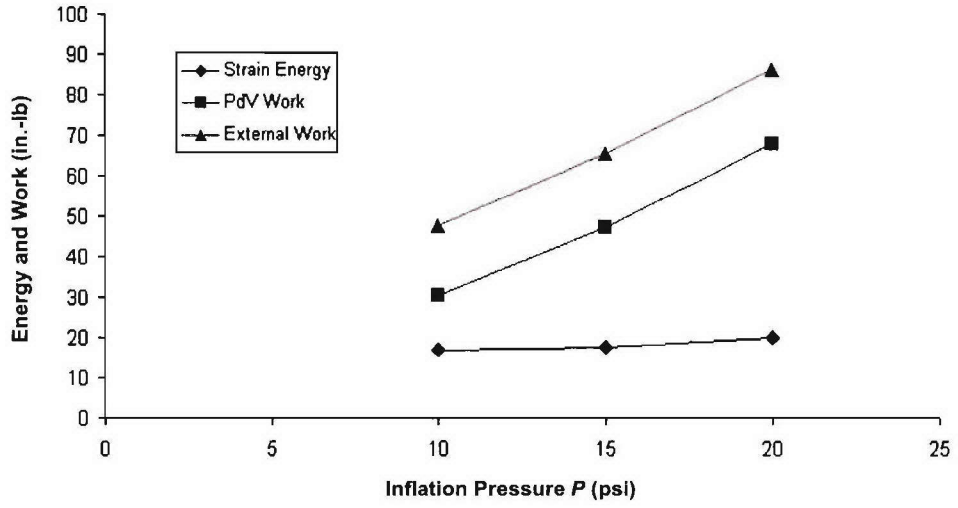

Figure 18. W_{ext}, ΔE_{strain}, and PdV-work vs P for a Hyperelastic Fabric: Reduced Polynomial (N = 3) Strain Energy Potential Applied with P at 10, 15, and 20 psi—Case 3

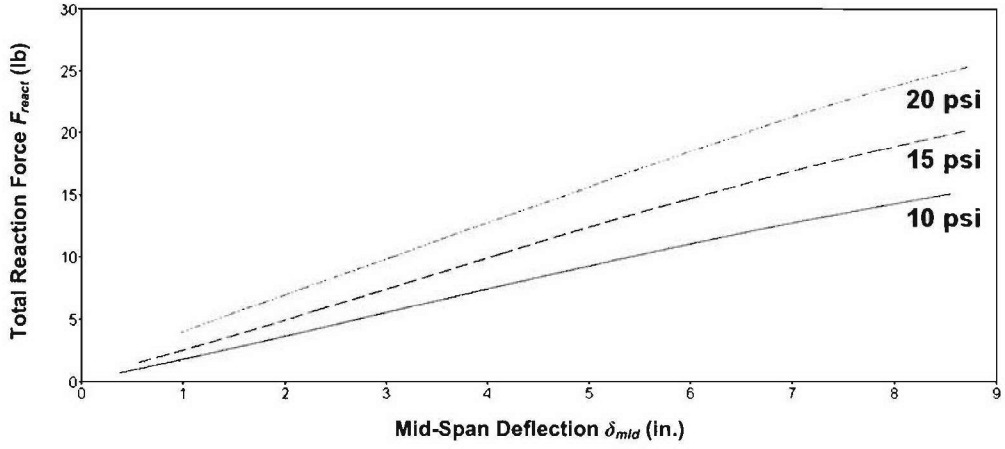

Figure 19. F_{react} vs δ_{mid} for Hyperelastic Fabric Model with P at 10, 15, and 20 psi—Case 3

Table 5. Summary of Pressure, Volume, and Energy Changes During Bending Step for the Hyperelastic Fabric Model—Case 3

P (psi)	ΔP (psi)	ΔV (in.^{3})	$\Delta \int PdV$ (in.-lb)	ΔE_{strain} (in.-lb)
10	0.052	-2.96	29.74	16.81
15	0.063	-3.13	46.94	17.54
20	0.073	-3.22	64.66	20.10

Time history curves of σ_{warp} on the outermost compressive surface at the mid-span are plotted in figure 20 for the inflation and bending steps for P at 10, 15, and 20 psi.

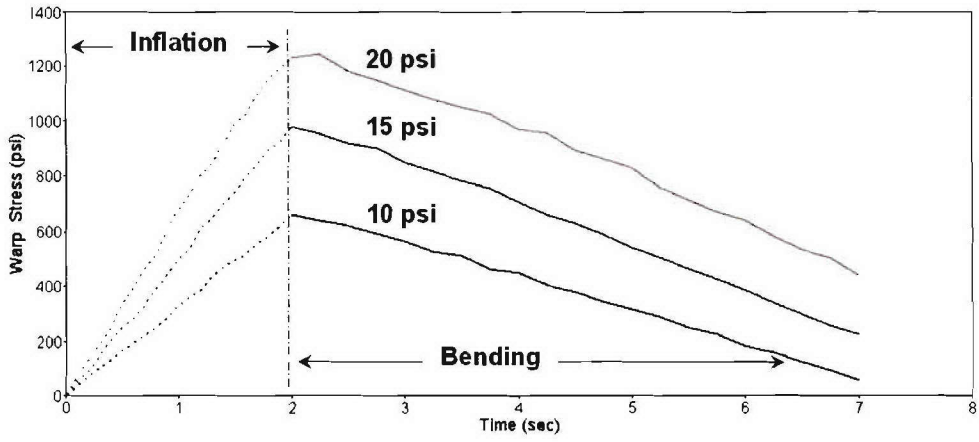

Figure 20. Time History Plot of σ_{warp} for Inflation and Bending Steps with P at 10, 15, and 20 psi—Case 3

Plots of σ_{warp} and σ_{weft} versus warp and weft strain, respectively, are shown in figure 21 for the inflation and bending steps at the mid-span, outermost compressive surface. Stresses due to inflation are designated with dashed lines, and stresses due to bending are designated with solid lines. Note that S during inflation is approximately 2:1, and only minimal changes in σ_{weft} occur during bending, particularly for P at 10 and 15 psi.

The treatment of the fabric constitutive behavior as a hyperelastic material is limited to those fabrics at stress levels in which the actual fabric shear modulus can be sufficiently represented by the strain energy potential.

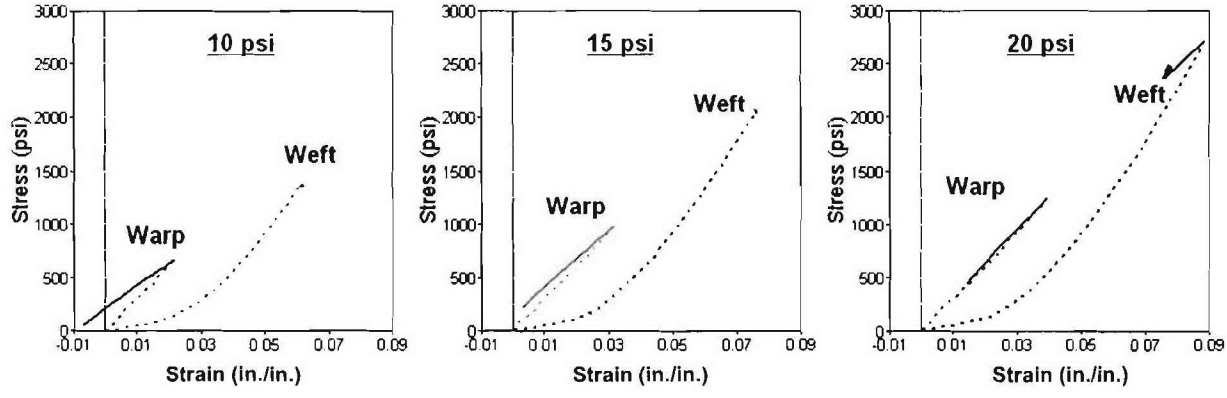

Figure 21. Plots of σ_{warp} and σ_{weft} vs Strain for P at 10, 15, and 20 psi—Case 3

DISCUSSION

The bending performance of plain-woven fabric air beams was investigated through a combined material-level test and finite element analysis approach. Using ABAQUS/Explicit, the fluid-structure interactions resulting from pressure-volume changes during inflation and four-point bending events were determined. The warp tensile stress-strain curve of the fabric was established from an equi-biaxial extension test and was used to formulate both linear elastic and hyperelastic constitutive cases for the air beam bending model.

The material-level tests confirmed that the plain-woven fabric did not behave as a continuum but rather as a discrete assemblage of fibers and yarns. For the range of pressures considered, E and G were independent of each other and were based on changes in fabric architecture (crimp interchange, yarn slip, rotation, etc.), *YDR*, and stress ratio S. Although E obtained from the biaxial warp stress-strain curve was highly nonlinear with P, it was monotonic with stress (and pressure) beyond 0.5 psi and was easily represented using a polynomial curve fit for input to the air beam models. However, G was not monotonic in γ. Three distinct regions developed in the plot of τ versus γ and were dominated by yarn rotations and shear jamming. Referring to figure 9, regions I and II were highly dependent on γ; and region II was expected to produce the largest ΔV in the plain-woven air beam models because of transverse shearing deformations from bending. During bending, this shear-induced ΔV was a source of *PdV-work*.

The material-level biaxial test was conducted in an equi-biaxial extension mode. As a consequence, S was not controlled, but it is hypothesized that, for an uncoated, plain-woven fabric subjected to equi-biaxial extension, the value of S for which convergence in ε occurs, denoted S^C, appears to be given by equation (5):

$$S^C = f\left(\frac{A_{weft}}{A_{warp}}, \zeta^{-1}, YDR\right). \tag{5}$$

To properly simulate the inflated air beam stress state in a swatch specimen, a combined biaxial and shear test fixture with the capacity to regulate a 2:1 biaxial tensile stress ratio is needed. Development efforts are underway to provide this experimental capability.

Comparisons were made between the fabric strain energy E_{strain} and *PdV-work* done on the air beam during bending. It was shown in linear elastic case 1 that E_{strain} dominated the bending behavior when $P < 30$ psi, so that ΔV and *PdV-work* were minimal. However, when $P \geq 90$ psi and ΔV was large, *PdV-work* dictated bending behavior, and the material constitutive effects (E_{strain}) on bending behavior were minimal. Results from linear elastic case 2 obtained for pressures up to 20 psi also showed that E_{strain} dominated the bending behavior. The hyperelastic case 3 results exhibited larger ΔV and *PdV-work* for the pressures of 10, 15, and 20 psi. However, E_{strain} contributed approximately 25% to the energy balance. In general, both terms—E_{strain} and *PdV-work* —must be determined for air beams subject to bending loads because γ will increase with decreasing pressure and lead to increasing values of ΔV.

The elastic and hyperelastic constitutive theories are of limited use if shearing deformations must be considered. These theories couple the extension and shear behaviors, which, on the contrary, were shown uncoupled through material-level tests. Consequently, the use of these theories is unlikely to capture the critical shear response (regions I and II in figure 9) and may lead to erroneous bending predictions. However, these theories may provide acceptable constitutive predictions for use in models of coated woven fabric air beams. Aside from the obvious environmental protections afforded by coatings, coatings provide additional elastic and shear stiffness by minimizing yarn slip and rotation. The added shear stiffness reduces shearing deformations, especially those developing in regions I and II. As a result, ΔV and *PdV-work* will be less in comparison to the same terms for uncoated fabric air beams. In the limiting case, the constitutive behavior of coated woven fabrics approaches that of matrix-reinforced fibrous composites.

If the fabric constitutive properties are nonlinear, the instantaneous tangent modulus, E'_{tan}, must be used at the corresponding stress state arising from the specific inflation pressure. However, if E'_{tan} and G change considerably with respect to pressure and bending loads, these moduli must be numerically updated in the models to properly assess bending behavior beyond simple perturbation states. Hence, the need exists to measure ΔV during air beam bending tests so that sufficient model validation can be performed.

CONCLUSIONS

It is concluded that, for a specific air beam deflection, the volume change will be larger at higher inflation pressures than for lower inflation pressures because the beam is stiffer at higher pressures and will require more external force to achieve the deflection. The higher external force creates larger shear forces in the beam, and, thus, a greater shear distortion occurs. Therefore, volume changes are expectedly greater with increasing inflation pressures for a prescribed deflection.

Air compressibility (*PdV-work*) introduces a nonlinear stiffening effect in the bending behavior of inflatable fabric structures. As the air volume decreases due to deformations from external loads (such as transverse shear, wrinkling, and section collapse), the air pressure will increase. The air behaves as a nonlinear spring, and its impact on bending behavior is directly related to ΔV. If air compressibility is appreciable, a gas law must be incorporated in the bending analysis.

REFERENCES

1. P. Cavallaro, A. Sadegh, and M. Johnson, "Mechanics of Plain-Woven Fabrics for Inflated Structures," *International Journal of Composite Structures*, vol. 61, no. 4, 2003, pp 375–393.

2. P. Cavallaro, C. Quigley, and A. Johnson, A. Sadegh, "Effects of Coupled Biaxial Tension and Shear Stresses on Decrimping Behavior in Pressurized Woven Fabrics," *2004 ASME International Mechanical Engineering Congress and Exposition*, Anaheim, CA, 13 November 2004, IMECE2004-59848.

3. Paul V. Cavallaro, Ali M. Sadegh, and Claudia J. Quigley, "Combined In-Plane Shear and Multi-Axial Tension or Compression Testing Apparatus," U.S. Patent No. 6,860,156, 1 March 2005.

4. "ABAQUS/Explicit," Version 6.4, ABAQUS Inc., Pawtucket, RI, 2003.

5. F. T. Pierce, *Journal of the Textile Institute*, vol. 28, T45, 1937.

6. "HyperWorks," Version 7.0, Altair Engineering, Inc., Troy, MI, 2005.

7. K. J. Bathe, *Finite Element Procedures in Engineering Analysis*, Prentice-Hall, Englewood Cliffs, NJ, 1982.

APPENDIX A
IDEAL GAS EQUATION OF STATE (EOS)

The ideal gas equation of state (EOS)* is given as

$$P + P_A = \rho R\left(\theta - \theta^Z\right), \tag{A-1}$$

where

P is the internal pressure,

P_A is the ambient pressure (14.7 psi),

ρ is the density of air (4.4274e-005 lb/in.^{3}),

R is the gas constant,

θ is the current temperature (21°C), and

θ^Z is the absolute zero temperature (-273.15°C).

The ideal gas constant R is given by

$$R = \widetilde{R} / M_w, \tag{A-2}$$

where

$\widetilde{R}$ is the universal gas constant $\left(2.841 \times 10^4 \dfrac{\text{lb in.}^2}{\text{mole s}^{2\circ}\text{K}}\right)$, and

M_w is the molecular weight (28.97 moles).

*"ABAQUS/Explicit," Version 6.4, ABAQUS Inc., Pawtucket, RI, 2003.

APPENDIX B
REDUCED POLYNOMIAL ($N = 3$) STRAIN ENERGY POTENTIAL

The reduced polynomial ($N = 3$) strain energy potential* is given as

$$U = \sum_{i=1}^{N} C_{i0}\left(\bar{I}_1 - 3\right)^i + \sum_{i=1}^{N} \frac{1}{D_i}\left(J^{el} - 1\right)^{2i}, \tag{B-1}$$

where

U = strain energy per unit volume,

N = material parameter,

C_{i0} = temperature dependent material parameter,

D_i = temperature dependent material parameter,

$\bar{I}_1$ = first deviatoric strain invariant, and

J^{el} = elastic volume ratio.

The initial shear modulus μ_0 is given by

$$\mu_0 = 2\left(C_{10} + C_{01}\right). \tag{B-2}$$

To define the limiting case, the fabric membrane elements were assumed to be fully incompressible by setting D_1, D_2, and D_3 to zero. The initial shear modulus, μ_0, was 507.2 psi. The constants C_{i1}, C_{10}, C_{20}, and C_{30} are given below:

$C_{i1} = C_{i2} = 0$ psi,
$C_{10} = 253.62$ psi
$C_{20} = 155{,}072.53$ psi, and
$C_{30} = 1{,}914{,}968.40$ psi.

*"ABAQUS/Explicit," Version 6.4, ABAQUS Inc., Pawtucket, RI, 2003.

INITIAL DISTRIBUTION LIST

Addressee	No. of Copies
U.S. Army Natick Soldier Center (R. Benny, J. Cullinane, G. Gildea, T. Godfrey, J. Hampel, K. Horak, M. Jee, F. Kostka, J. Miletti, C. Quigley, J. Roche, M. Roylanc, K. Santee, G. Thibault)	14
Army Research Laboratory, Langley (MS-188E –A. R. Johnson, J. Chen)	2
Army Research Laboratory, Aberdeen (AMSRD-ARL-WM-MD – R. Dooley, B. Cheeseman, D. Granville)	3
U.S. Army Engineer Research and Development Center, Coastal and Hydraulics Laboratory (D. Resio, J. Melby, J. Fowler)	3
U.S. Army Research Office (AMSRD-ARL-RO-EN – A. Rajendran, G. Anderson, B. LaMattina)	3
Office of Naval Research (ONR 334 – R. Barsoum)	1
Naval Surface Warfare Center, Carderock Division, W. Bethesda, MD (Code 21 – A. Rausch)	1
Naval Surface Warfare Center, Carderock Division, Norfolk, VA (Code 23 – D. Jacobson)	1
Center for Naval Analyses	1
The City College of New York, New York, NY (A. Sadegh)	5
Northeastern University, Boston, MA (J. N. Rossettos, H. Nayeb-Hashemi)	2
University of Massachusetts – Dartmouth, North Dartmouth, MA (S. Warner)	1
University of Massachusetts – Lowell, Lowell, MA (J. Meade)	1
Federal Fabrics-Fibers Inc., Lowell, MA (F. Guerts)	1
ILC–Dover, Frederica, DE (J. Welch, D. Cadogan)	2
Vertigo Inc., Lake Elsinore, CA (G. Brown, D. Jorgensen, R. Haggard)	3
Warwick Mills, New Ipswich, NH (C. Howland)	1
Defense Technical Information Center	2